Sustainable Cities and Society 94 (2023) 104537

Contents lists available at ScienceDirect

Sustainable Cities and Society

journal homepage: www.elsevier.com/locate/scs

Effects of Vertical Forests on Air Quality in Step-up Street Canyons

Geon Kang [a], Jae-Jin Kim [b,*]

[a] Supercomputer Center, Pukyong National University, Busan, Korea
[b] Division of Earth and Environmental System Sciences, Pukyong National University, Busan, Korea

ARTICLE INFO

Keywords:
CFD model
dry deposition parameterization
Step-up street canyon
tree effects
vertical forest

ABSTRACT

Vertical forests have been constructed as environmentally friendly solutions for air quality and urban heat problems. With an expectation to provide insights into the value of vertical forests, we examined the impact of these structures on flows and distribution of fine particles in step-up street canyons using a computational fluid dynamics (CFD) model. The CFD model was rigorously validated against wind-tunnel experiments and accurately simulated particle deposition efficiency by tree leaves under varying wind speed and leaf area density (LAD) conditions, as well as the flow structures in step-up street canyons. We analyzed the characteristics of flows and fine particle distributions in step-up street canyons for different LADs and tree deposition velocities. Despite a substantial reduction in fine particles through dry deposition, the fine particles emitted from two line-type sources within the street canyon increased by 20-25% in the canyon's lower layer due to a 14-20% reduction in wind speed. This study sheds light on the complex flow structures and pollutant distributions surrounding vertical forests and highlights the need for a comprehensive evaluation and optimal design of these structures.

1. Introduction

The International Agency for Research on Cancer, which is a member agency of the World Health Organization, classifies air pollution and fine particulate matter (PM) as Group 1 carcinogens (Loomis et al., 2013). In addition, the public's understanding of the dangers posed by fine dust has increased. Smaller PM grains remain in the air longer, which increases the risk of inhalation and deposition deep in the respiratory system. Moreover, long-term exposure to PM causes diseases such as asthma, lung disease, and cardiovascular disease (World Health Organization, 2006, Mukherjee and Agrawal, 2017). Accordingly, various approaches to reduce PM and improve air quality are being established nationally and internationally, along with fundamental solutions to PM control such as pollution-source regulation and reduced reliance on coal to reduce fine dust (McNabola et al., 2013; Gallagher et al., 2015; Irga et al., 2015; Mukherjee and Agrawal, 2017; Hewitt et al., 2020; Su et al. 2021).

One approach to reducing PM is to create green infrastructure, such as urban forests or green spaces, as part of urban planning (Hewitt et al., 2020). Trees provide city dwellers with healthy indoor and outdoor living conditions by improving air quality and by ameliorating the thermal environment through evapotranspiration (Gago et al., 2013; Irga et al., 2015; Chen et al. 2021). Green infrastructure has contributed to improving the sustainability of cities worldwide. For instance, Stuttgart, Germany, has a long-standing tradition of incorporating green spaces such as parks and green roofs into its urban design (Claus and Rousseau, 2012; Irga et al., 2017), which has been shown to improve air quality and reduce the urban heat island effect. To enhance the quality of air, mitigate the urban heat island effect, and promote overall sustainability, similar plans for green infrastructures (street tree planting, green roofs, and park development) have been implemented in New York, Tokyo, Hong Kong, and Singapore (Foster et al., 2011; Aflaki et al., 2017; Irga et al., 2017; Kumar et al. 2019).

In densely populated metropolitan areas that often lack green and open spaces, trees can be planted on building roofs and walls in addition to planting them in the ground. Recently, Stefano Boeri's project gave a birth of a new type of architecture in which vegetation is vertically planted in cantilevered balconies on the exterior walls of buildings, creating a so-called vertical forest (Boeri, 2015). A representative example of a vertical forest is the Bosco Verticale in Milan, Italy. About 800 trees and tens of thousands of other plants were vertically planted around the building, providing about 30,000 m^2 of green space on a building site of about 3,000 m^2 (Boeri, 2015), establishing a large area of green space in a small area of the inner city. This successful creation of a vertical forest within a limited area has been followed by several new vertical projects in recent years, including the 'Vertical Forest' in Italy,

* Corresponding author at: Division of Earth and Environmental System Sciences, Pukyong National University, 45, Yongso-ro, Nam-Gu, Busan 48513, Korea.
E-mail address: jjkim@pknu.ac.kr (J.-J. Kim).

https://doi.org/10.1016/j.scs.2023.104537
Received 15 November 2022; Received in revised form 18 February 2023; Accepted 14 March 2023
Available online 24 March 2023

'Park Royal on Pickering' in Singapore, 'Tao Zhu Yin Yuan' in Taiwan, 'Easyhome Huanggang Vertical Forest' in China, 'Planeta Building' in Spain, 'ACROS Fukuoka' in Japan, 'Nanjing Vertical Forest' in China, and 'One Central Park' in Australia. More are expected to be established in the future.

Trees can be thought of as porous obstacles that decrease the speed of air flow as wind passes through their leaves by reducing the dynamic pressure. Densely planted trees provide excellent protection against strong flows by reducing flow speeds downwind of their canopies by more than 50%. Trees therefore act as effective windbreaks and provide shelter in areas that experience frequent strong winds (Bird, 1998; Brandle et al., 2004). However, trees can potentially reduce air quality in areas with frequent weak winds (Gromke et al., 2008), which has led to research into the effects of trees on air quality in typical urban street canyons, including sources of pollution. Although green infrastructure has been proposed as a solution to improve air quality in urban areas, several previous studies have shown that the impact of green infrastructure on air quality is very complex and depends on the layout of buildings and trees. Gromke et al. (2008) showed that trees in the center of a street canyon increase (decrease) pollutant concentrations at the wall surface of the upwind (downwind) building. Vos et al. (2013) conducted an experiment that analyzed 19 different vegetation design scenarios along roadsides, with the majority leading to a decline in air quality. Santiago et al. (2017) found that while vegetation has a deposition effect reducing pollutant concentrations near roadsides, it increases concentrations in heavily trafficked streets by reducing ventilation. Barwise and Kumar (2020) noted the potential harm from biogenic volatile organic compounds (BVOCs) and pollen emitted in large quantities by certain plants in green infrastructure and emphasized the importance of choosing appropriate vegetation for each site. In street canyons, the distribution of pollutants depends on surrounding conditions such as building and street aspect ratios, pollutant source locations, wind speeds, and wind directions. Abhijith et al. (2017) have also shown that trees and hedges can affect air quality in street canyons when the surrounding conditions are otherwise the same. The impact of green infrastructure on air quality is intricate and influenced by multiple factors, including the characteristics of the urban environment and vegetation. Hence, more in-depth studies are necessary to comprehend vegetation's role in enhancing or deteriorating air quality.

This study aimed to investigate the effects of vertical forests on pollutant dispersion in step-up street canyons. A step-up street canyon is defined as a street canyon whose height of the upwind building is smaller than the downwind building. We analyzed the complicated interaction between vegetation and air quality, emphasizing the significance of considering the aerodynamic and deposition effects in reducing pollutant concentrations. For this, we performed numerical simulations of pollutant dispersion using a computational fluid dynamics (CFD) model with a dry deposition parameterization scheme. The fine-particle concentrations simulated by the CFD model were validated against those measured in a wind tunnel by Huang et al. (2013). The CFD model was then applied to the simulations of air flows and pollutant dispersion in step-up street canyons with the same building configurations as those in Addepalli and Pardyjak (2013). To determine the effects of vertical forests on air flows and pollutant dispersion, we considered the potential configurations in which vertical forests could be established on the walls and roofs in the step-up street canyons. Section 2 describes the CFD model with dry deposition parameterization schemes and presents the validation results. The simulation results of air flows and pollutant dispersion are analyzed in section 3, and the results and conclusions are given in section 4. The findings in this study can hopefully inform urban planners, architects, and environmental scientists about designing and implementing more effective green infrastructures and contribute to developing sustainable solutions for improving air quality in urban areas.

2. Numerical model description

2.1. Computational fluid dynamics model

The CFD model used in this study was the same as that used in Kang et al. (2020). The model originated from a non-commercial CFD model developed by Argonne National Laboratory (Lee and Park, 1994). This model has been continuously improved through previous studies (Baik and Kim, 1999; Kim and Baik, 1999; Kim and Baik, 2004; Baik et al., 2007; Kim et al., 2012; Park et al., 2016; Kang et al., 2017). The CFD model was based on unsteady (time dependent) Reynolds-averaged Navier–Stokes equations, which assume a three-dimensional, non-hydrostatic, non-rotating, Boussinesq airflow system. The renormalization group (RNG) k-ε turbulence closure scheme suggested by Yakhot et al. (1992) was employed for turbulence parameterization. The governing equations were numerically solved using a finite volume method in a staggered grid system and the semi-implicit method for pressure-linked equations (SIMPLE) algorithm (Patankar, 2018). To reflect the effects of the turbulent boundary layer near the solid wall surfaces, we implemented the wall boundary conditions suggested by Versteeg and Malalasekera (1995).

Trees decrease wind speed by reducing dynamic pressure, and consequently, they can change the production rate of turbulence kinetic energy (TKE, k) and TKE dissipation (ε) (Ries and Eichhorn, 2001; Balczó et al., 2009). To account for the pressure loss caused by trees, Kang et al. (2017) implemented tree parameterization terms (Green, 1992; Ries and Eichhorn, 2001; Balczo et al., 2009) in the equations of momentum, TKE (k), and TKE dissipation rate (ε) as follows:

$$\left.\frac{dU_i}{dt}\right|_{tree} = \left.\frac{dU_i}{dt}\right|_{org} - n_c^3 \cdot c_d \cdot LAD \cdot U_i \cdot |\boldsymbol{U}|. \tag{1}$$

$$\left.\frac{dk}{dt}\right|_{tree} = \left.\frac{dk}{dt}\right|_{org} + n_c^3 c_d LAD |\boldsymbol{U}|^3 - 4 n_c^3 c_d LAD k |\boldsymbol{U}|. \tag{2}$$

The second last (source) and last (sink) terms of the right-hand side in equation 2 indicate the conversion of mean kinetic energy into TKE and the cascade of TKE from large to small scales by tree leaves, respectively. Based on the Kolmogorov relation (Launder and Spalding, 1974), the source and sink terms in equation 2 are associated with those in the equation of the TKE dissipation rate:

$$\left.\frac{d\varepsilon}{dt}\right|_{tree} = \left.\frac{d\varepsilon}{dt}\right|_{org} + \frac{3}{2}\frac{\varepsilon}{k} n_c^3 c_d LAD |\boldsymbol{U}|^3 - 6 n_c^3 c_d LAD \varepsilon |\boldsymbol{U}|. \tag{3}$$

Here, the subscripts *tree* and *org* indicate the prognostic equations with and without the parameterization terms of the tree's drag, respectively. The stand density, n_c, indicates the area fraction of the vertically projected tree coverage and ranges from 0 (no tree) to 1 (full tree coverage in the grid cell), and c_d is the leaf-drag coefficient. The leaf area density (LAD) is defined as the total one-sided leaf area per unit volume. U_i is the i^{th} mean velocity component (i = 1, 2, 3), and $|\boldsymbol{U}|$ represents wind speed. For further details, see Kang et al. (2020).

In this study, we added the parameterization term for dry deposition on tree leaves to the equation of pollutant transport. Dry deposition is parameterized by means of a downward flux in the last term of the transport equation as follows (Zhang et al., 2001, Neft et al., 2016):

$$\frac{\partial C}{\partial t} + U_j \frac{\partial C}{\partial t} = D \frac{\partial^2 C}{\partial x_j \partial x_j} - \frac{\partial}{\partial x_j}\left(\overline{cu_j}\right) - LAD \cdot V_d \cdot C. \tag{4}$$

Here, C is the mean concentration of a given pollutant species in air and D is the molecular diffusivity of the pollutant. V_d is the dry deposition velocity. For details about V_d, see Zhang et al. (2001) and Neft et al. (2016). The factors c and u_i are fluctuations from the respective means of C and U_i. The turbulent flux of pollutants, $-\overline{cu_j}$, is parameterized in terms of grid-resolvable variables as follows:

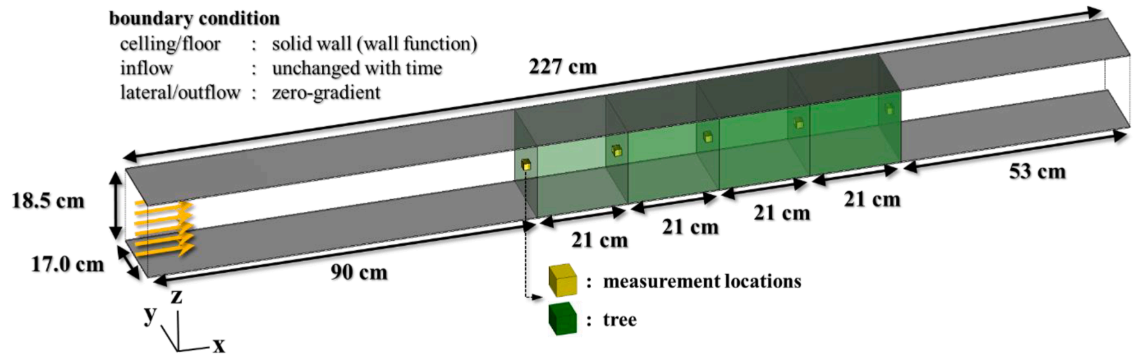

Fig. 1. Overview of the numerical configuration for validation against the wind-tunnel experiment of Huang et al. (2013).

Table 1
Summary of leaf area density (LAD), inflow wind speed, and drag coefficient (c_d) used in three LAD scenarios.

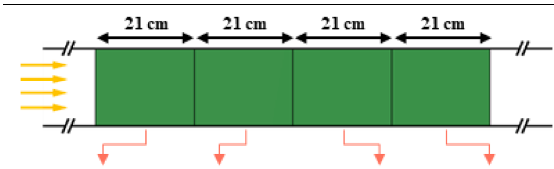

	x (cm)	0-21	21-42	42-63	63-84
LAD ($m^2\ m^{-3}$) scenario	uniform	263	263	263	263
	increasing	176	241	307	371
	decreasing	405	334	262	191
inflow wind speed scenario	low	0.3 m s^{-1} with c_d = 0.46			
	medium	0.6 m s^{-1} with c_d = 0.40			
	high	0.9 m s^{-1} with c_d = 0.35			

$$-\overline{cu_j} = K_c \frac{\partial C}{\partial x_j}. \tag{5}$$

Here, the eddy diffusivity of the pollutant concentration, K_C, is determined by the eddy diffusivity of momentum (ν_t) and turbulent Schmidt number (Sc_t) ($K_C = \nu_t / Sc_t$). The eddy diffusivity of momentum is defined as $\nu_t = C_\mu\ k^2/\varepsilon$ [here, C_μ (= 0.0845) is the empirical constant of the RNG $k - \varepsilon$ turbulence closure scheme, and Sc_t is 0.9]. For details about V_d, see Zhang et al. (2001) and Neft et al. (2016).

2.2. Model validation

We previously validated simulated results against empirical measurements from wind tunnel and field experiments to verify the accuracy of tree drag parameterization as implemented in the CFD model (Kang et al., 2017 and 2020). The pollutant concentrations simulated with the drag parameterization scheme approximated those measured by Gromke et al. (2008). The statistical validation indices of the pollutant concentrations simulated on both the upwind and downwind walls in street canyons were comparable to those simulated by a large-eddy simulation (LES) model (Moonen et al., 2013). In addition, the CFD model accurately reproduced the wind speeds and TKEs measured in field experiments by Kurotani et al., (2001). The root-mean-square errors (RMSEs) for wind speeds and TKEs were comparable to those simulated by the LES model in Qi and Ishihara (2018). Both of these validation exercises implied that the CFD model could successfully implement realistic drag parameterizations. Further details of these validations can be found in Kang et al. (2017, 2020).

In this study, we conducted a validation of the dry deposition scheme implemented in the CFD model by comparing the simulated particle deposition efficiency with particle deposition measured in wind-tunnel experiments by Huang et al. (2013). For comparison, we conducted simulations in the same configuration as Huang et al. (2013) (Fig. 1). The numerical domain measured 227 cm in length (x-direction), 17 cm in width (y-direction), and 18.5 cm in height (z-direction). The grid sizes were uniform (0.5 cm) in three directions, and the numbers of cells were 454, 34, and 37 in the x-, y-, and z-directions, respectively. Trees were filled from x = 90–174 cm, and particle concentrations were detected at five points (every 21 cm from x = 90 cm).

We considered three scenarios using different LAD distributions with downwind distance: uniform LAD, linearly increasing LAD, and linearly decreasing LAD (Table 1). For each LAD scenario, we conducted simulations using three inflow wind speeds: low (0.3 m s^{-1}), medium (0.6 m s^{-1}), and high (0.9 m s^{-1}). Leaf-drag coefficients of 0.46, 0.4, and 0.35 corresponded to inflow wind speeds of 0.3, 0.6, and 0.9 m s^{-1}, respectively (Neft et al., 2016). The particle diameters were set from 5 nm to 95 nm at intervals of 5 nm, which yielded 19 diameter classes.

Figure 2 shows the relationship between the particle deposition efficiency and the cumulative leaf area index (LAI) for different inflow speeds in the LAD scenarios. LAI was defined as $LAI = \int_0^x LAD(x)dx$, and the particle deposition efficiency was averaged over the complete range of particle diameters. The deposition efficiency was proportional to the cumulative LAD but varied inversely with the wind speed. The CFD model reproduced measured deposition efficiency in the uniform and increasing LAD scenarios for low and medium wind speeds better than for the decreasing LAD scenario. The CFD model overestimated deposition efficiencies in the uniform and increasing LAD scenarios for high wind speeds but underestimated it in the decreasing LAD scenario. These results were similar to those of Huang et al. (2013). The CFD model overestimated the penetration of small (< 50 nm) particles in the decreasing LAD scenario, which contributed to underestimating the measured deposition efficiency.

Because information on particle diameters was lacking in the measurements, we averaged deposition efficiency over the 19 particle diameters. The correlation coefficient (R) between measured and simulated particle deposition efficiencies was close to 1.0, and the fraction of predictions within a factor of 2 was 1.0. The RMSE was comparable to that reported by Huang et al. (2013). These results demonstrated that the deposition parameterization scheme implemented in the CFD model reproduced the measured efficiency of particle deposition with reasonable accuracy. We therefore investigated the drag and deposition effects of vertical forests on flows and particle concentrations in step-up street canyons using the same building configurations as Addepalli and Pardyjak (2013) and Park et al. (2020).

2.3. Simulation setup

We used the same step-up street canyon configuration as the one used in wind tunnel measurements by Addepalli and Pardyjak (2013) and simulations by Park et al. (2020) (Fig. 3). The street-canyon width was 32 m (S), the height of the upwind building (building A) was 57.6 m

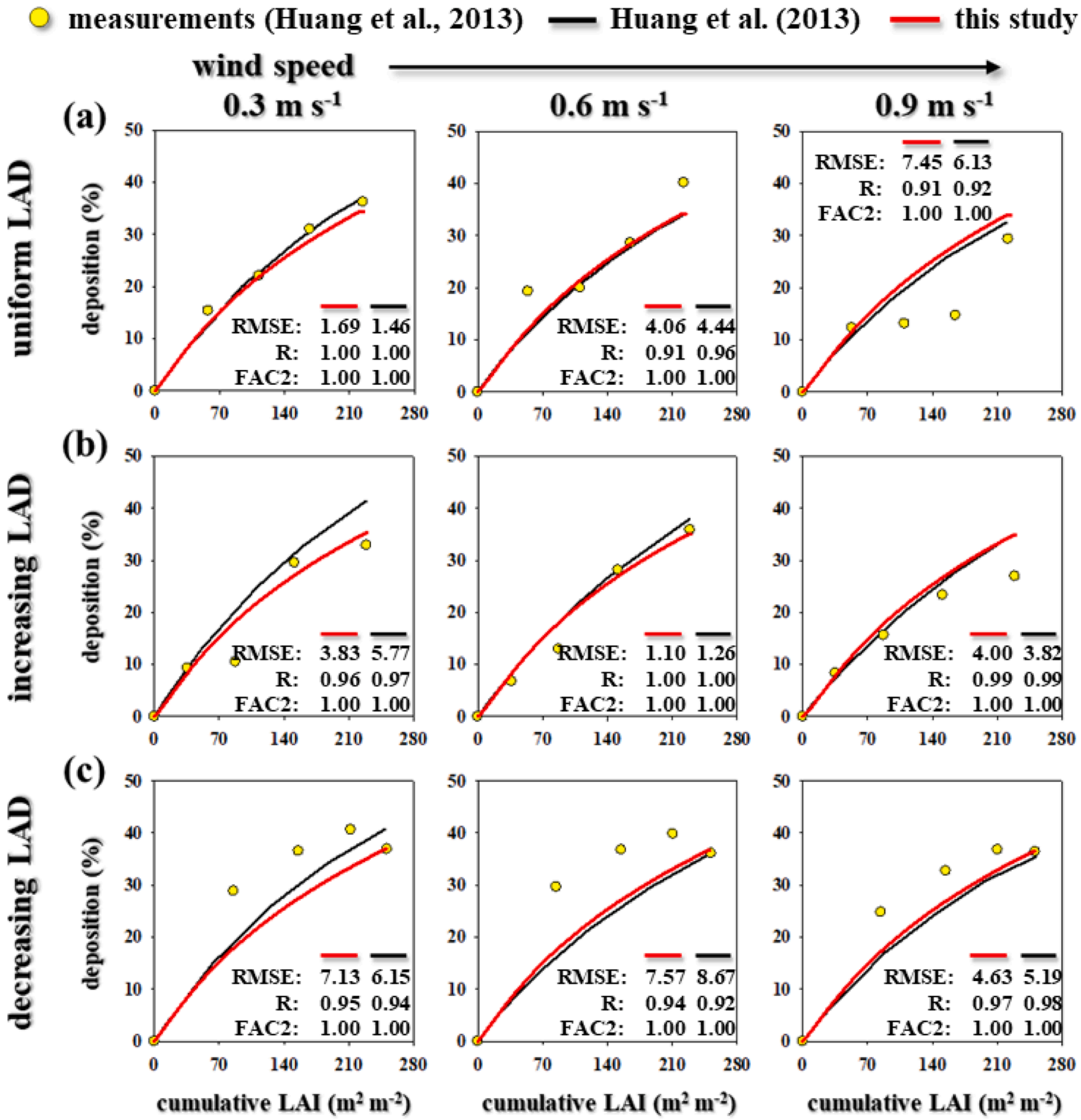

Fig. 2. Comparison of particle deposition efficiency in this study using measured and simulated deposition from Huang et al. (2013) in the (a) uniform, (b) increasing, and (c) decreasing LAD scenarios for low (left), medium (middle), and high wind speeds (right).

(1.8 S), the height of the downwind building (building B) was 96 m (3 S), and the length of the buildings was 96 m (Fig. 3a). The grid sizes were 1.6 m in the all three directions, and there were 360 cells in the x-direction, 260 in the y-direction, and 180 in the z-direction. We conducted additional simulations with different grid resolutions to see whether the CFD model depended on grid size in simulating the step-up street canyon flows in the absence of trees. The results showed no marked difference in flow pattern with increasing grid sizes (Fig. A1).

Figure 3b shows the top, side, and three-dimensional views of the step-up street canyon with a vertical forest. The configuration of the vertical forest in this study was motivated by the vertical forest in Milan, Italy consisting of 800 trees (480 large trees and 300 small trees) and approximately 15,000 plants. In the CFD simulations, trees and plants were represented by parameters linked to leaf attributes, such as LAD, n_c, c_d, and V_d. We assumed that trees existed up to a distance of 3.2 m from the walls and roof. The tree-planting rate per grid was about 50%, and c_d was 0.2 (the average value of urban vegetation) (Gromke and Blocken, 2015; Buccolieri et al., 2018). The investigation of the impact of LAD on flow and pollutant dispersion was conducted by considering four cases with LADs of 0.5, 1.0, 1.5, and 2.0 m^2 m^{-3}, which encompass the LAD ranges of various tree and vegetation species observed in the vertical forest. The deposition velocity (V_d) ranges from 0.1 to several cm s^{-1}, depending on the vegetation and pollutant species, as well as the particle size (Buccolieri et al., 2018; Giardina and Buffa, 2018). For each LAD case, we set deposition velocities from 0.0 to 3.0 cm s^{-1} in 0.2-cm s^{-1} increments. The deposition velocities considered in this study lay within the range of those for ultrafine particles (< 0.1 μm in diameter) and fine particles (< 2.5 μm in diameter) (Vos et al., 2013; Buccolieri et al., 2018; Giardina and Buffa, 2018). We assumed that non-reactive pollutants (fine particles) were emitted at a rate of 10 g s^{-1} from line-type sources located at the center of the first grid cells from the ground within the street canyon (red lines in Fig. 3a). The vertical profiles of wind, TKE, and the TKE dissipation rate at the inflow boundary were specified by equations 6–10:

$$U(z) = U_B\left(\frac{z}{H_B}\right)^{\alpha}, \tag{6}$$

$$V(z) = 0, \tag{7}$$

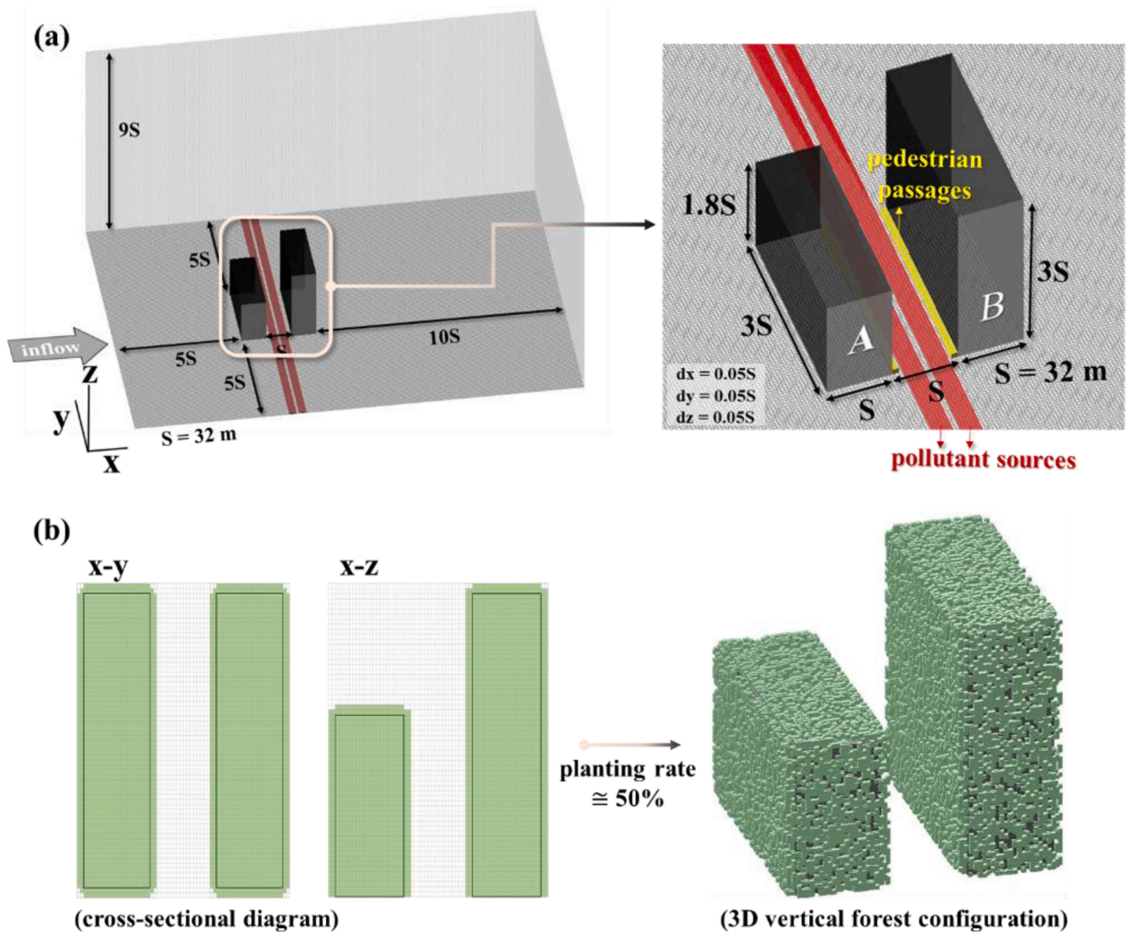

Fig. 3. (a) The numerical domain and building configuration considered in this study, and (b) top, side, and three-dimensional views of the step-up street canyon with a vertical forest. Trees are planted on the exterior walls and roofs of buildings.

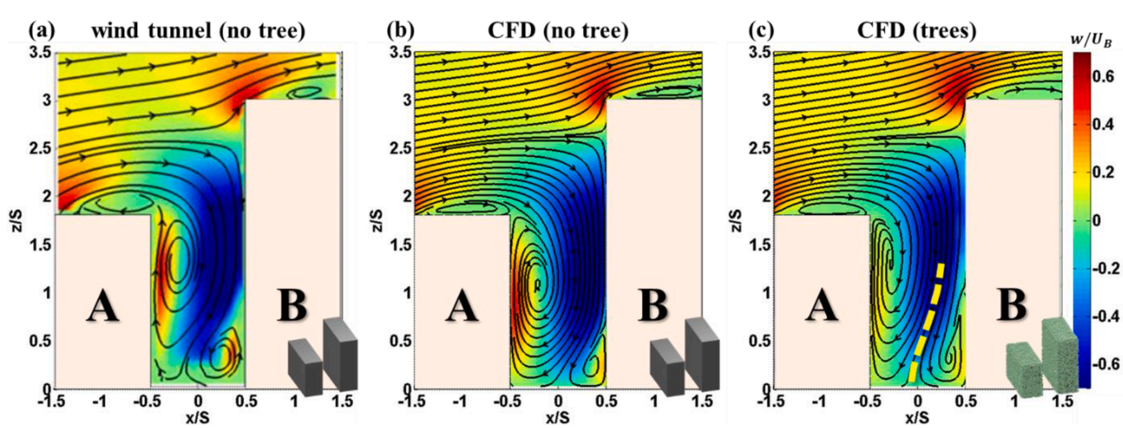

Fig. 4. Streamlines and contours of the vertical wind components at the canyon center (y/S = 0) (a) measured by Addepalli and Pardyjak (2013) and simulated in (b) the absence of and (c) presence of trees in this study. The vertical wind components were normalized by $U_B = 4.32$ m s^{-1}.

$$W(z) = 0, \tag{8}$$

$$k(z) = \frac{1}{C_\mu^{1/2}} U_*^2 \left(1 - \frac{z}{\delta}\right)^2, \tag{9}$$

$$\varepsilon(z) = \frac{C_\mu^{3/4}\, k^{3/2}}{\kappa z}. \tag{10}$$

where U_B is wind speed at the downwind building height (4.32 m s^{-1}), $H_B = 96$ m, and the power-law exponent (α) is 0.21. The constants C_μ, U_*, δ, and κ represent the empirical constant (0.09), friction velocity (0.26 m s^{-1}), boundary layer depth (1000 m), and von Kármán constant (0.4), respectively. The CFD simulations were numerically integrated, with a time step of 0.5 s, up to 3600 s when the mean fields reached the quasi-steady state.

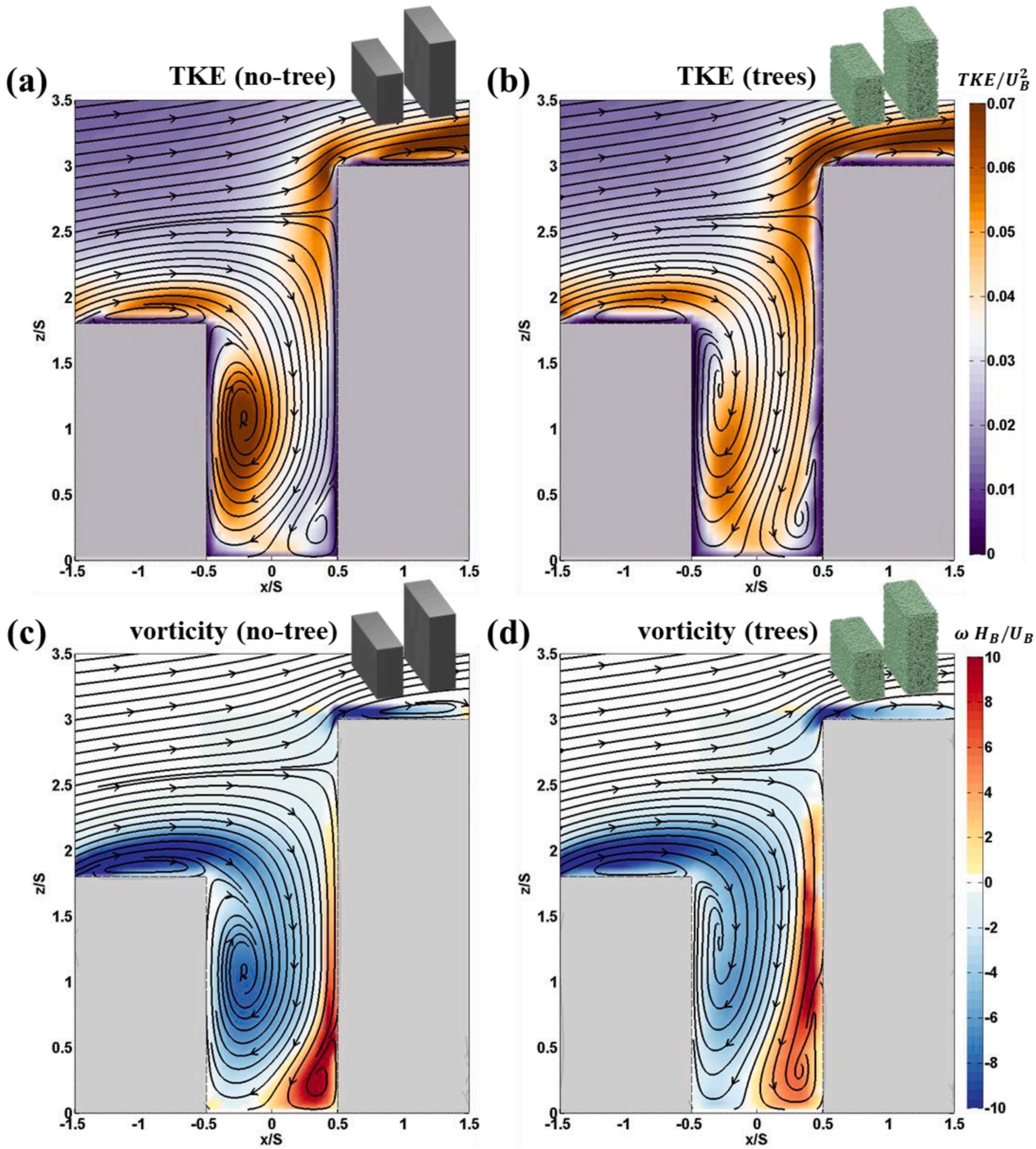

Fig. 5. Streamlines and contours of TKE (upper panel) and vorticity (lower panel) in the (a and c) absence of and (b and d) presence of trees. TKEs and vorticities were normalized by U_B^2 and U_B/H_B, respectively.

3. Results and discussion

3.1. Flow characteristics

First, we examined how well the CFD model reproduced the flow structures measured in the wind tunnel by Addepalli and Pardyjak (2013). We then investigated the effects of vertical forests on flow patterns in the step-up street canyon. Figure 4 shows the measured and simulated streamlines and contours of the vertical wind components at the canyon center (y/S = 0). For comparison, the vertical wind components were normalized by U_B (4.32 m s^{-1}). Measured airflows collided with building B (Fig. 4a), forming a stagnation point. The airflow separated around the stagnation point, with one part descending the wall of building B (WB) and the other part ascending. The descending flow further separated around the street-canyon center close to ground level. Part of this separated flow proceeded toward building A and contributed to the formation of the primary vortex in the street canyon. Another part of the separated flow went toward building B and formed the corner vortex. Meanwhile, other flows separated from the leading edge of building A and B to form rooftop recirculation zones.

In the absence of trees, the CFD model reproduced measured flow structures such as the primary and corner vortices and the rooftop recirculation zones but underestimated the magnitude of the corner vortex and rooftop recirculation zones (Fig. 4b). Descending and ascending flows below and above the stagnation point became weaker in the presence of trees because of the drag exerted by the trees planted on WB. The near-wall attenuation in flow speed increased the velocity gradient along WB (Fig. 4c). Subsequently, the vortices inside the canyon changed in intensity and shape. Overall, the updraft and downdraft of the primary and corner vortices were weakened, the center of the primary vortex shifted slightly toward the upper left, and the corner vortex increased in size.

The inclusion of a vertical forest on the buildings significantly changed the in-canyon TKE and vorticity ($\omega = \frac{\partial W}{\partial x} - \frac{\partial U}{\partial z}$) distributions

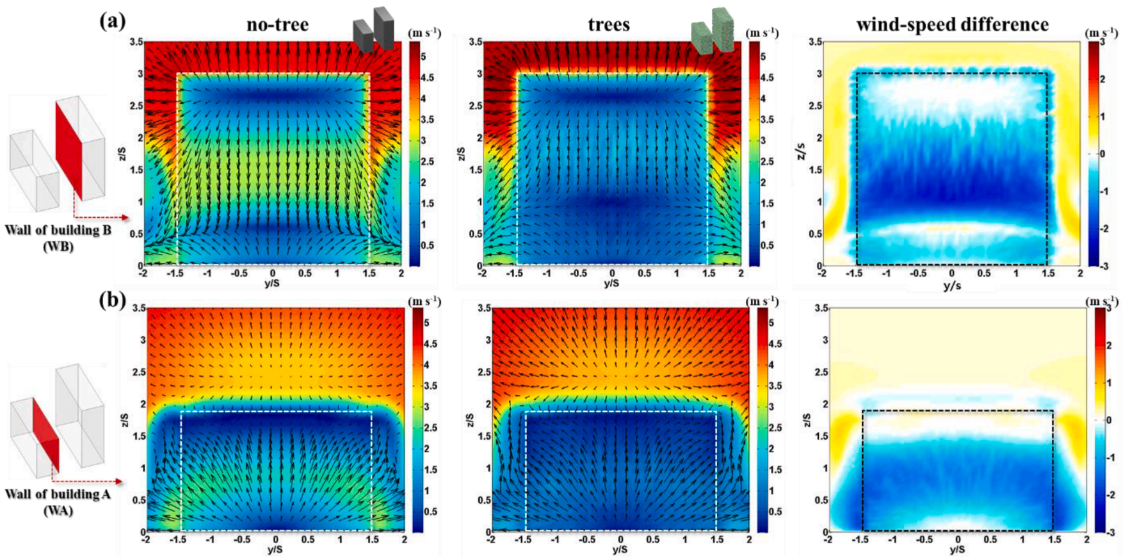

Fig. 6. The wind vectors and the contours of wind speeds and wind-speed differences near (a) building B (x/S = 0.475) and (b) building A (x /S = −0.475) in the absence and presence of trees.

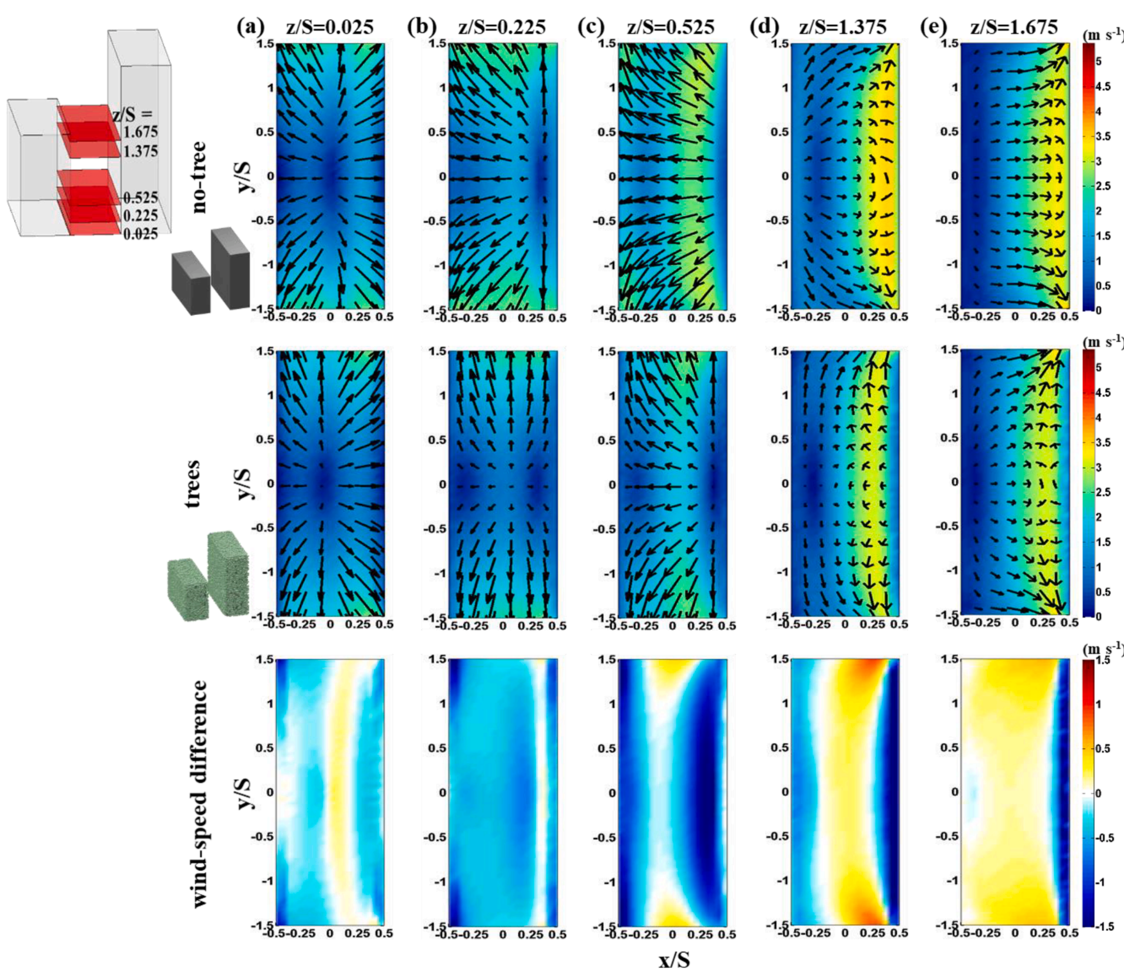

Fig. 7. The wind vectors and the contours of the wind speeds and wind-speed differences at z/S values of (a) 0.025, (b) 0.225, (c) 0.525, (d) 1.375, and (e) 1.675 in the absence and presence of trees.

(Fig. 5). The trees decreased the TKEs over the central and updraft parts of the primary vortex (Figs. 5a and 5b). The decrease in TKE was caused by the reduction in velocity gradient within the primary vortex, which in turn was caused by decreased updraft wind speeds near building A and a reduced downdraft between the primary and corner vortices (yellow dashed line in Fig. 4c). The reduction in velocity gradient also weakened

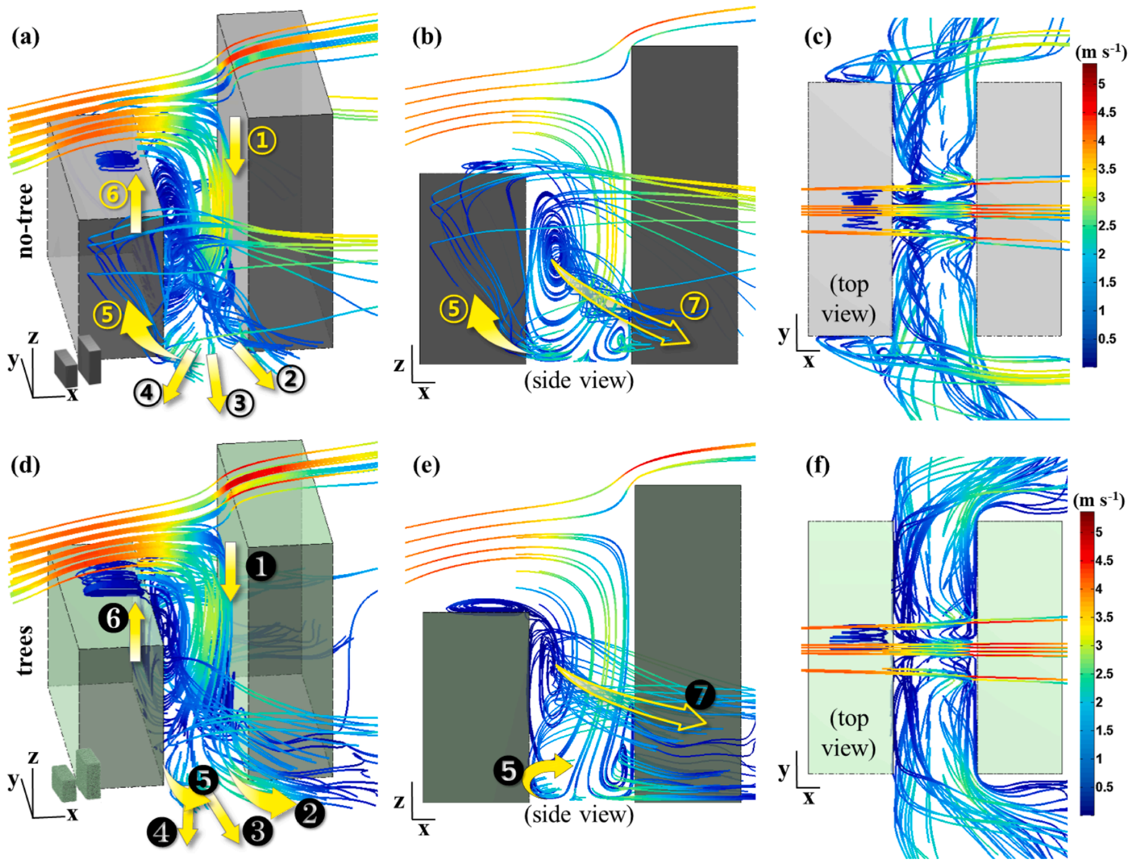

Fig. 8. Three-dimensional (left panel), side (middle panel), and top (right panel) views of streamlines around the step-up street canyon in the (a, b, and c) absence of and (d, e, and f) presence of trees.

the negative vorticity within the primary vortex (Figs. 5c and 5d). By contrast, trees increased the TKEs near building B and over the downdraft components of the primary and corner vortices. The weakened near-wall and among-vortices downdrafts contributed to increased velocity gradients and TKEs in the surrounding areas. Compared with the no-tree case (Fig. 5c), the maximum vorticity near the center of the corner vortex decreased slightly, and positive vorticity extended widely, even to the stagnation point (Fig. 5d). As a result, the primary vortex decreased, while the corner increased, in size. Similar vortex changes due to roughness or vegetation on building exterior walls have been reported in previous studies (Fellini et al., 2020; Li et al., 2022). The vortex structure change inside the step-up street canyon was more significant than in the even-notch street canyon (Li et al., 2022).

We analyzed changes to within-canyon flow characteristics in detail. Figure 6 shows the wind vectors and contours of the wind speeds and wind-speed differences near the wall of building A (WA) and WB in the absence and presence of trees. The airflow colliding with WB diverged upward, outward, and downward at the stagnation points near $z/S = 2.6$. The downdraft dominated between the stagnation points and a convergence zone corresponding to the upper boundary of the corner vortex. The trees on WB weakened the near-wall downdraft, the updraft of the corner vortex, and the outward flows near the WB's edge. The significant reduction of the downdraft in the presence of trees induced the rise of the convergence zone up to $z/S = 1.0$, compared to $z/S = 0.5$ in the absence of trees. The airflow diverged upward and outward near WA. In the presence of trees, the speeds of the diverged flows decreased overall, an effect that principally occurred below $z/S = 1.5$ and near the lateral boundaries of the street canyon.

Trees caused significant changes in flow patterns with height (Fig. 7). Divergence zones and the boundaries of the primary and corner vortices, at $z/S = 0.025$, 0.225, and 0.525, moved toward building A (Figs. 7a–7c). Trees also induced a divergence of the flow near building B at $z/S = 1.375$ (Fig. 7d), which implied horizontal and vertical growth of the corner vortex. Although the outward flows strengthened, the reverse flow became weak, resulting in reduced wind speeds in the low levels (Figs. 7a–7c). The streamwise flow in the upper part of the primary vortex also weakened slightly, but trees contributed to greater within-canyon wind speeds by strengthening outward flows in the higher levels (Figs. 7d and 7e). The movement of the divergence zone toward building A resulted in increased wind speeds ($0.0 \leq x/S \leq 0.2$) at $z/S = 0.025$ (Fig. 7a).

Figure 8 summarizes the flow characteristics around the step-up street canyon in the absence and presence of trees. In the absence of trees (Figs. 8a–8c), the airflows above building A collided with building B, inducing a downdraft along WB (① in Fig. 8a). Figures 8a and 8b illustrate the divergence of the downdraft near the ground, after which one part flowed out of the street canyon (②, ③) and the other moved toward building A (i.e., reverse flow). The reverse flow diverged near WA, inducing outward flow near the ground (④), upward flow through the side-wall recirculation (⑤; refer also to Fig. 8 in Park et al., 2020), and an updraft along WA (⑥). The primary vortex laterally extended to the outside of the canyon, forming a portal vortex through which a part of the airflow flowed to the outside of the canyon (⑦).

The vertical forest significantly changed the size and intensity of flow structures within the primary and corner vortices (Figs. 8d–8f). The primary vortex became small while the corner vortex grew vertically. The intensity of the vortices decreased due to the drag exerted by the trees. Trees weakened the downdraft (❶ in Fig. 8d) and near-ground outflows through the lateral boundaries of the street canyon (❷, ❸, ❹ in Figs. 8d and 8e). In the presence of trees, the side-wall recirculation and upward flow (⑤ in Fig. 8a) beside building A disappeared. Instead, the outward flow near building A (❺ in Fig. 8d) was directed toward the

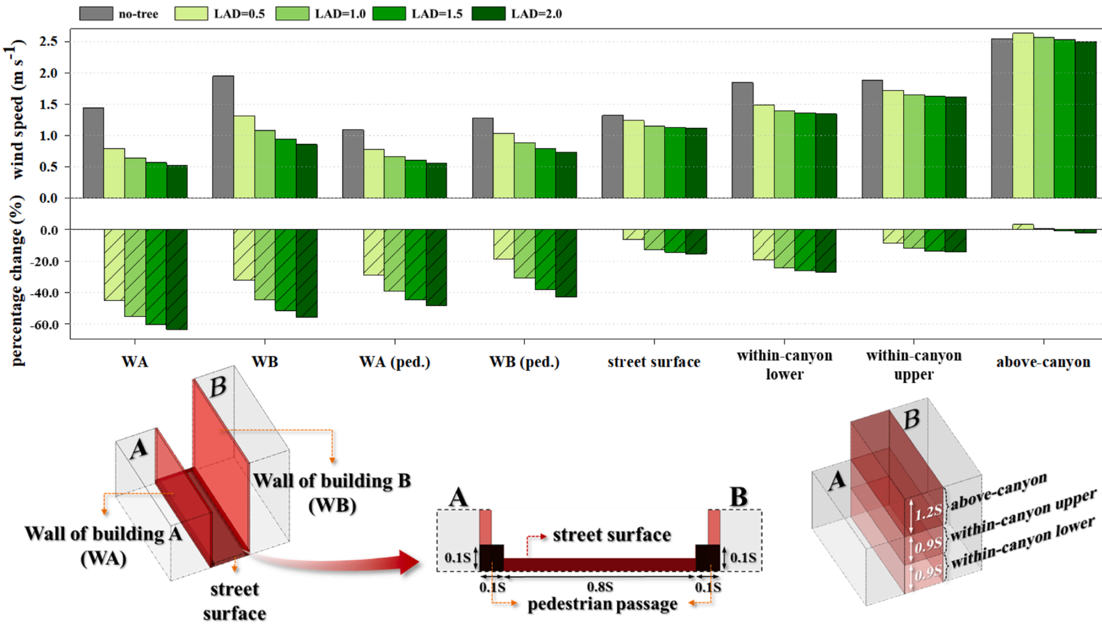

Fig. 9. Average wind speeds and wind reduction rates on the inner surfaces of the street canyon (WA, WB, and street surface) and three layers: within-canyon lower layer ($0 < z/S \leq 0.9$), within-canyon upper layer ($0.9 < z/S \leq 1.8$), and above-canyon layer ($1.8 < z/S \leq 3.0$). The percentage change was defined as the percentile rate of increase or decrease in average wind speed caused by trees divided by the average wind speed in the no-tree case.

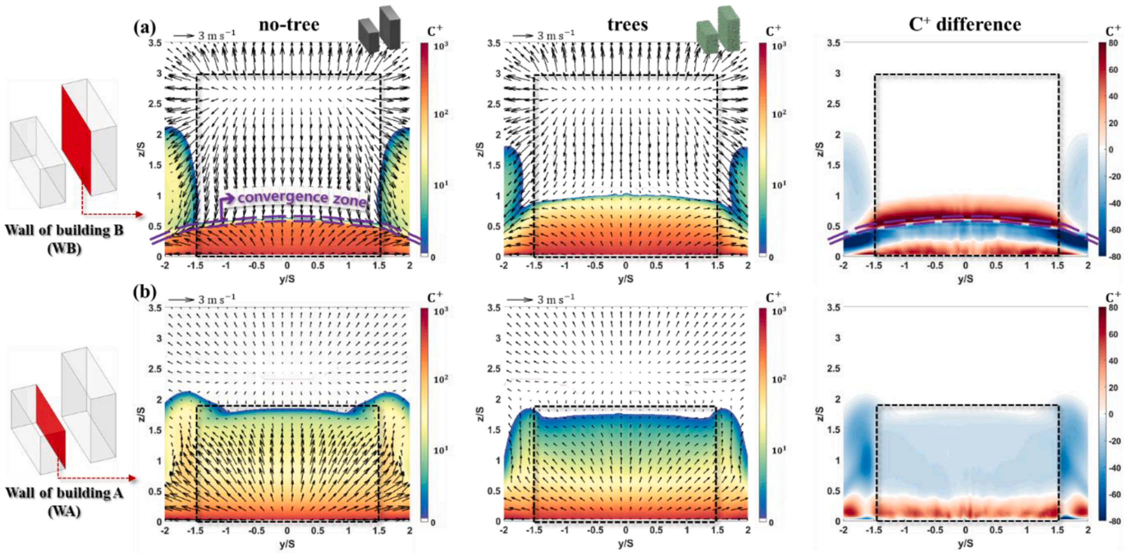

Fig. 10. Wind vectors and contours of the dimensionless concentrations (C^+) and C^+ differences near (a) building B ($x/S = 0.475$) and (b) building A ($x/S = -0.475$) in the absence and presence of trees.

downwind region just after escaping from the street canyon. In the absence of trees, the side-wall recirculation resulted from detouring of the inflow toward building A (Tominaga and Stathopoulos, 2016; Park et al., 2020). However, trees on the side wall of building A reduced the reverse flow of the side-wall recirculation, increased TKE and turbulent diffusivity of momentum, made the detoured flow permeate the near-wall region of building A, and therefore hampered growth of the side-wall recirculation. As the side-wall recirculation disappeared, the detoured flows approached the street canyon and directed outward flows from the street canyon in the streamwise direction. The airflow through the portal vortex formed a wider outflow from the street canyon than it did in the absence of trees (❼ in Fig. 8e).

These results indicate the degree of accuracy with which the CFD model reproduced the measured flow structure in a step-up street canyon and described in detail how a vertical forest could change flow structures. We also analyzed how the LAD of the vertical forest influenced average wind speeds over street-canyon surfaces (WA, WB, and the street surface) and in three layers: within-canyon lower layer ($0 < z/S \leq 0.9$), within-canyon upper layer ($0.9 < z/S \leq 1.8$), and above-canyon layer ($1.8 < z/S \leq 3.0$) (Fig. 9). Trees reduced near-wall and within-canyon average wind speeds in proportion to LAD. Wind-speed reduction was maximized on WA (e.g., 63.6% at LAD = 2.0) and minimized at the street surface (6–15%) (Fig. 9a). However, wind-speed reductions became significant in both the upwind (48.5%) and downwind (43.1%) pedestrian pathways at LAD = 2.0. Within-canyon wind speeds were reduced by approximately 14–20%, with the greatest reduction in the within-canyon lower layer being about twice the reduction in the within-canyon upper layer. However, above-canyon

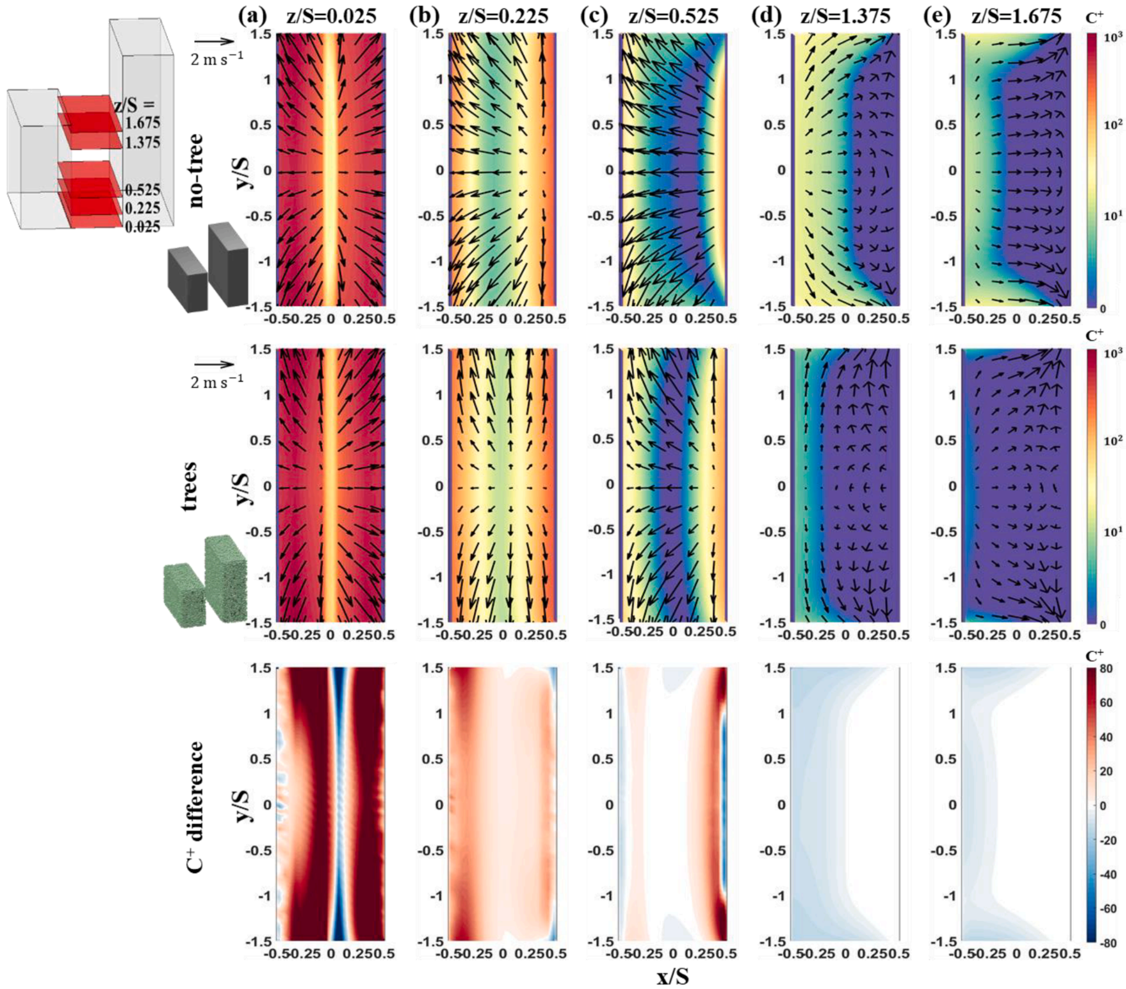

Fig. 11. Wind vectors and contours of the dimensionless concentrations (C^+) and C^+ differences at z/S = (a) 0.025, (b) 0.225, (c) 0.525, (d) 1.375, and (e) 1.675 in the absence and presence of trees.

wind speeds increased slightly at LAD ≤ 1.0 (Fig. 9b).

3.2. Dispersion characteristics

We investigated the distributions of non-reactive fine particles with diameters of less than 2.5 μm in the absence and presence of trees around the step-up canyon. Figure 10 shows the wind vectors and contours of the dimensionless fine-particle concentrations (C^+) and differences in C^+ between WA and WB. The variable $C^+ = CU_BH_B^2/Q_l$, where C is the fine-particle concentration and Q_l is the total emission rate. We assumed that the LAD of trees was 1.0 $m^2\ m^{-3}$ and that the V_d of fine particles was 1 cm s^{-1}.

In the absence of trees, fine-particle concentrations were high near the ground on both WA and WB. This distribution of fine particles occurred because they were directed from their emission source toward WA and WB by the primary and corner vortices. On WB, steep gradients of fine-particle concentration occurred along the convergence zone of the downdrafts and updrafts, with low and high concentrations, respectively. On WA, fine particles were transported up to the roof level by the updrafts of the primary vortex. In the presence of trees on WB, the convergence zone moved upward (the vertical growth of the corner vortex), and fine particles reached the convergence zone. In the absence of trees, the vertical extension of the fine-particle distribution allowed fine-particle concentrations to increase above the convergence zone (violet dashed line in Fig. 10a) and decrease below it (violet dashed line in Fig. 10a). Reduced wind speeds (Fig. 9) increased fine-particle concentrations near the ground on WB in the presence of trees.

On WA, fine-particle concentrations increased near the ground (z/S ≤ 0.5) and slightly decreased at z/S $\gtrsim$ 0.5 in the presence of trees. In the absence of trees, fine particles reached the roof level outside WA (y/S ≥ |1.5|) due to the side-wall recirculation, and they were also transported to the outside of WB (y/S ≥ |1.5|). In the presence of trees, the side-wall recirculation and its pumping of fine particles disappeared, which decreased concentrations outside of the street canyon.

The vertical forest significantly changed the distribution of fine-particle concentrations but not their overall pattern (Fig. 11). Concentrations were high at z/S = 0.025 (close to the road emission) and z/S = 0.225, except near the street-canyon center, a region of the downdraft with low concentration, significantly increasing due to the wind-speed reduction caused by the vertical forest (Figs. 11a and 11b). At z/S = 0.525, the high-concentration region near WB extended toward the street-canyon center due to the growth of the corner vortex (Fig. 11c). In the presence of trees, concentrations decreased in the within-canyon upper layer (z/S = 1.375 and 1.675), despite the concentration increase in the within-canyon lower layer (Figs. 11d and 11e). The outward flows at z/S = 0.025 and 0.225 were enhanced by the vertical forest and transported more fine particles to the outside of the street canyon. These outward flows contributed to the concentration decreases at z/S $\gtrsim$ 0.5 on WB (Fig. 10) and at z/S = 1.375 and z/S = 1.675.

We examined the effects of LAD on the dimensionless concentrations ($\overline{C^+}$) averaged over eight sections of the street canyon: WA, WB, WA and WB pedestrian passages, street surface, within-canyon lower layer,

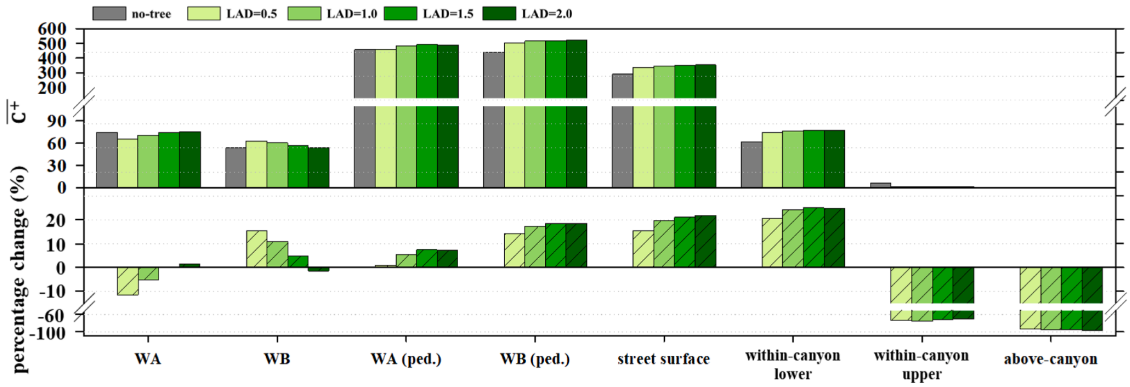

Fig. 12. The dimensionless concentrations ($\overline{C^+}$) averaged over the inner surfaces of the street canyon (WA, WB, and street surface) and three layers: within-canyon lower layer ($0 < z/S \leq 0.9$), within-canyon upper layer ($0.9 < z/S \leq 1.8$), and the above-canyon layer ($1.8 < z/S \leq 3.0$). The percentage change was defined as the percentile rate of $\overline{C^+}$ caused by trees to $\overline{C^+}$ in the no-tree case.

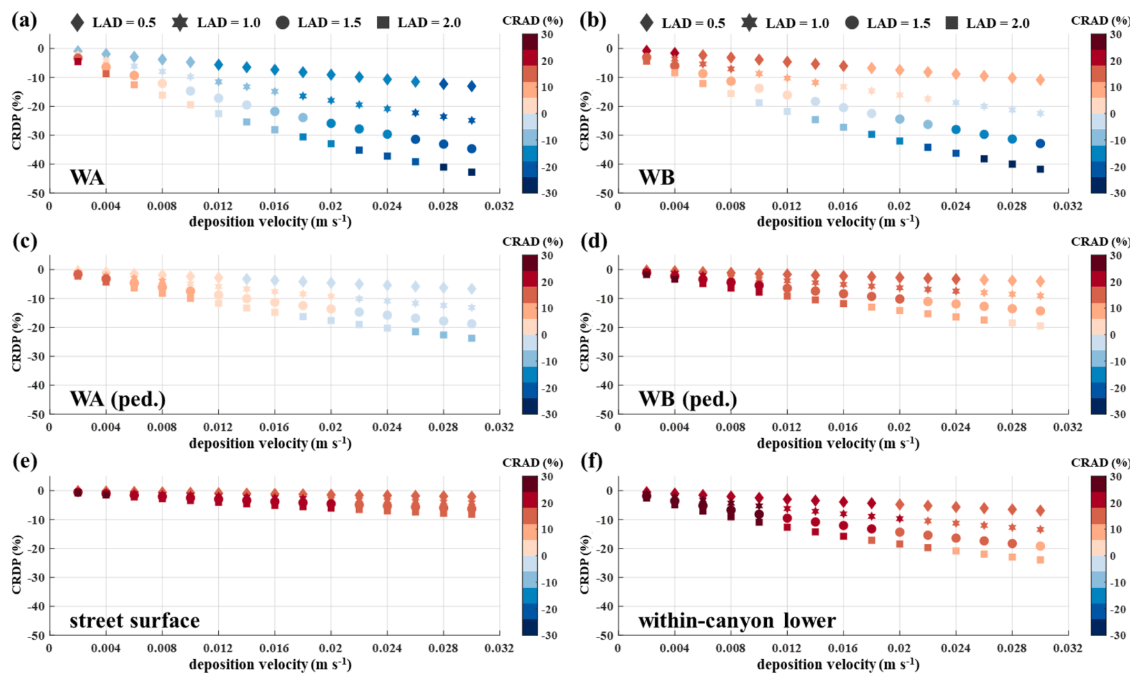

Fig. 13. The CRDP (%) and CRAD (%) for each LAD and V_d on (a) WA and (b) WB, and in the (c and d) pedestrian regions, (e) street surface, and (f) within-canyon lower layer.

upper layer, and the above-canyon layer in Fig. 9 (Fig. 12). Regardless of LAD, the vertical forest increased $\overline{C^+}$ in the pedestrian passages near WA and WB, at the street surface, and in the within-canyon lower layer. This result came about because average wind speeds were inversely proportional to LAD (Fig. 9). In the within-canyon lower layer, average wind speeds were 73–81% of those in the absence of trees, and $\overline{C^+}$ increased by 20–25%. The increase in pollutant concentration proportional to LAD was also derived in green infrastructure scenarios (Gromke et al., 2008; Vos et al., 2013; Abhijith et al., 2017). However, $\overline{C^+}$ in WB decreased as LAD increased. The increase of LAD resulted in the vertical growth of the corner vortex, and consequently induced a wide spread of particles in the corner vortex and extensive deposition on the leaves of trees on WB. The nonlinear combination of the trees' drag and dry deposition resulted in the nonmonotonic variation of $\overline{C^+}$ with the increase in LAD.

Next, we investigated the extent to which trees in the vertical forest contributed to reducing fine-particle concentrations (Fig. 13). To accomplish this, we conducted additional experiments at deposition velocities of 0.0–3.0 cm s^{-1} at 0.2-cm s^{-1} increments. We calculated the concentration rates changed by the deposition process (CRDP) and by aerodynamic (i.e., drag) and deposition processes (CRAD) using equations 11 and 12:

$$\mathrm{CRDP}\ (\%) = \frac{\overline{C^+_{\mathrm{tree}}} - \overline{C^+_{\mathrm{tree},\ V_d=0}}}{\overline{C^+_{\mathrm{tree},\ V_d=0}}} \times\ 100, \tag{11}$$

$$\mathrm{CRAD}\ (\%) = \frac{\overline{C^+_{\mathrm{tree}}} - \overline{C^+_{\mathrm{no-tree}}}}{\overline{C^+_{\mathrm{no-tree}}}} \times\ 100. \tag{12}$$

where $\overline{C^+_{\mathrm{no-tree}}}$ and $\overline{C^+_{\mathrm{tree}}}$ indicate $\overline{C^+}$ in the absence and presence of trees, respectively, and $\overline{C^+_{\mathrm{tree},\ V_d=0}}$ is $\overline{C^+}$ at a deposition velocity (V_d) of 0, indicating the case with the tree drag parameterization and without the deposition process.

CRDP was inversely proportional to LAD up to −42.7% on WA and −41.7% on WB. Values of CRAD were dominantly negative (that is, concentrations were reduced by trees) on WA, except at $V_d \leq 0.01$ m s^{-1}

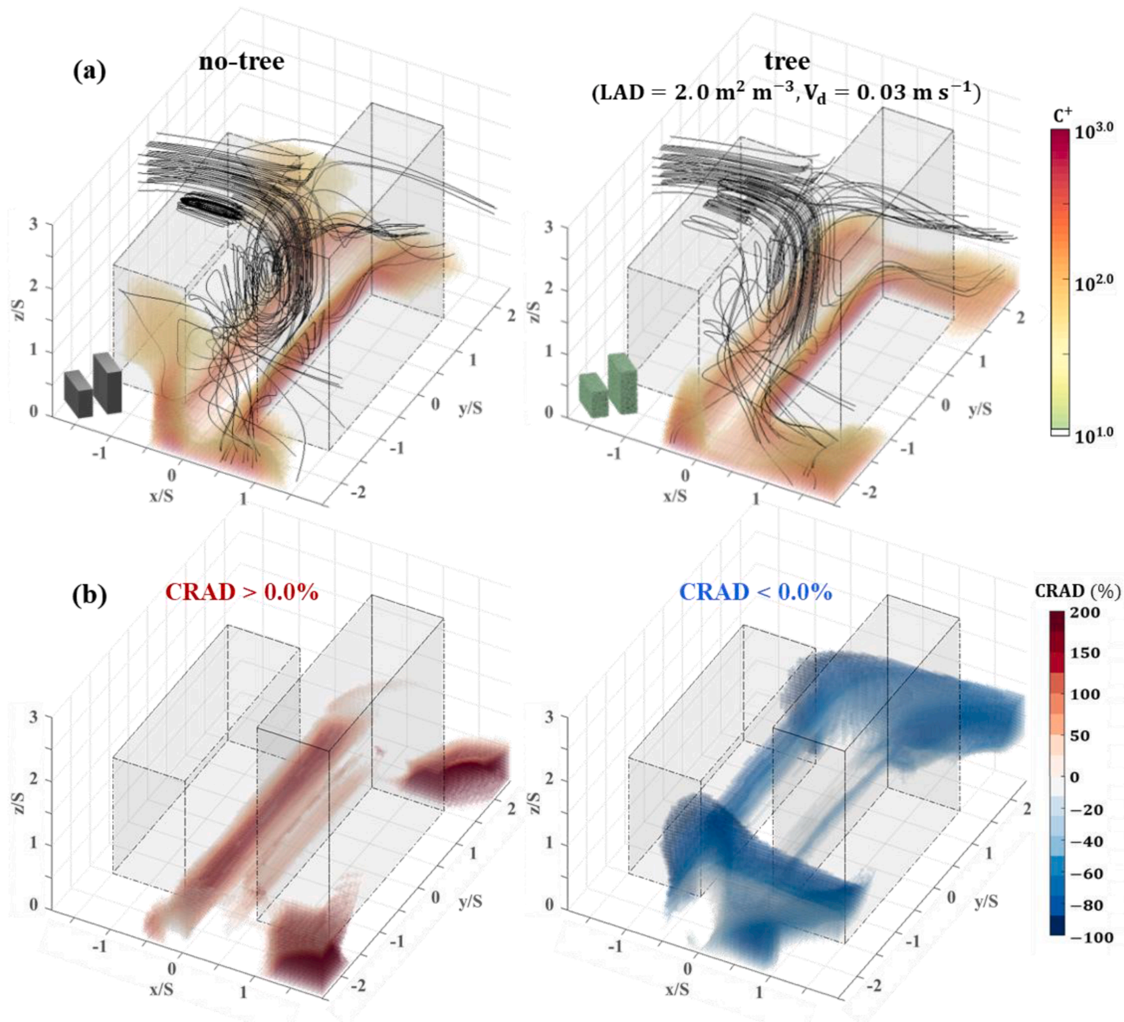

Fig. 14. The three-dimensional distributions of (a) the dimensionless concentrations, C^+, and (b) positive and negative CRADs around the step-up street canyon.

and LAD ≤ 1.0 or 1.5 (Fig. 13a). On WB, CRADs were positive at CRDPs ≤ −17.4% (Fig. 13b), implying that concentration reductions due to deposition were proportionately larger than concentration increases caused by reductions in wind speed. On WB pedestrian passage, the street surface, and the within-canyon lower layer, CRADs were always positive (Figs. 13c–13f), meaning that the concentration increase induced by aerodynamic processes was greater than the corresponding decrease produced by dry deposition processes in the low layer of the street canyons.

Figure 14 summarizes the characteristics of fine-particle distributions around the step-up street canyon in the absence and presence of trees. At the street-canyon center, fine-particle concentrations were relatively low due to the low concentrations in the downdraft (① in Fig. 8a). A portion of the fine particles was transported toward upwind and downwind buildings along the portal and corner vortices. Some of these particles were also transported outside the street canyon via outward airflows (②–⑦ in Figs. 8a and 8b). Trees decreased near-wall and within-canyon wind speeds, weakened or eliminated the side-wall recirculation (⑤ in Fig. 8b), and increased the size of the corner vortex. Fine particles emitted from the street surface were not transported to the upper-canyon layer as much as they were in the absence of trees. Instead of being transported toward the side-wall recirculation, fine particles were transported outside the street canyon through the outward flow (❺ in Fig. 8e) near the upwind building (Fig. 14a).

Despite the considerable reduction of fine particles through dry deposition and their direct outward transport (❷, ❸, ❹ in Fig. 8d), fine-particle concentrations increased in the lower layer of the street canyon because of reduced wind speeds in the portal vortex. This result is similar to that of Santiago et al. (2017). Because of nonlinear interactions between factors promoting increased (wind-speed reduction) and decreased (dry deposition) fine-particle concentrations (Zhang et al., 2020), it was difficult to judge whether the vertical forest decreased fine-particle concentrations in the street canyon. Meanwhile, CRAD enabled us to derive intuitive deductions about the effect of tree cover on fine-particle concentrations. Based on the CRAD distributions, trees increased fine-particle concentrations principally in the within-canyon lower layer, indicating the vertical forest's potential to increase fine-particle exposure to pedestrians except in WA. It also decreased concentrations in the upper layer within and outside the street canyon, implying the vertical forests' benefit to surrounding areas in fine-particle concentrations (Fig. 14b).

4. Summary and conclusions

We investigated the effects of vertical forests on air flows and pollutant dispersion in step-up street canyons. To achieve this, we implemented the dry deposition parameterization scheme in a CFD model, which was validated against empirical data obtained using a wind tunnel. Comparisons with the results of wind-tunnel measurements and previous simulations showed that the CFD model used in this study reproduced measured particle deposition efficiencies with reasonable accuracy. We used the CFD model to investigate the effects of trees on fine-particle flows and dispersal in step-up street canyons with and without vertical forests. We conducted simulations in the absence of trees to investigate the accuracy with which the CFD model reproduced the measured flow characteristics of the chosen building configuration. We then conducted simulations at LADs of 0.5–2.0 m^2 m^{-3} in 0.5-m^2 m^{-3} increments and deposition velocities of 0.0–3.0 cm s^{-1} in 0.2-cm s^{-1} increments. The CFD model without trees accurately reproduced the primary and corner vortices in the street canyon as well as the recirculation zones above and beside buildings.

We then investigated the airflow characteristics and fine-particle distributions in the presence of the trees in the simulated step-up street canyons. The vertical forest significantly changed flow patterns, TKE, and vorticity, principally by decreasing average wind speeds in the street canyon. Trees weakened the downdraft near the downwind building wall (WB), thereby increasing the velocity gradient and TKEs along WB. The trees also decreased the updraft near the upwind building wall (WA) and the velocity gradients and TKEs around the primary vortex. The center of the primary vortex slanted slightly toward building A and the corner vortex grew vertically. Average wind speeds in the within-canyon lower layer were reduced by 14–20%, and the greatest reductions in the average wind speed (up to 63.6%) were observed near WA.

We examined distributions of non-reactive pollutants (fine particles) around the step-up canyon in the absence of trees. The fine particles emitted from two separate line sources were transported toward the upwind and downwind building by the portal and corner vortices. Fine particles flowing toward the upwind building were transported to the roof level by updrafts from the primary vortex, into the side-wall recirculation, and to the outside of the street canyon through the lateral boundary. Fine particles flowing toward the downwind building concentrated inside the corner vortex. In the presence of trees, fine particles emitted from the street surface were not transported to the upper-canyon layer as much as they were in the absence of trees. Despite the considerable reduction of fine particles due to dry deposition and direct escape from the street canyon near the upwind building, fine-particle concentrations increased in the lower layer of the street canyon because of reduced wind speeds in the portal vortex and outward flows. The trees of the vertical forest principally increased fine-particle concentrations in the within-canyon lower layer and decreased concentrations in the upper layer inside and outside of the street canyon.

Vertical forests offer several advantages (exchanging carbon dioxide and oxygen, improving air quality, decreasing energy consumption in buildings, and alleviating the urban heat island effect). However, when implementing a vertical forest as a green infrastructure solution, it is required to consider both the cost and sustainability implications. Also, wind speed reduction by vertical forests may negatively affect ground-level air quality, highlighting the significance of proper placement and design of these structures. Hopefully, this study will clarify the understanding of the complicated flow structures and pollutant distributions in step-up street canyons with vertical forests.

However, it should be noted that this study was conducted under idealized street canyon configurations, ignoring the detailed and realistic designs because of the computational resource limitations. Further research is needed to understand the effect of vertical forests on air quality in different urban environments and under varying conditions. In future research, we will further investigate the effects of vertical forests on air quality using scenarios that account for background fine-particle concentrations and emissions. Further the following studies will be conducted shortly regarding vertical forests and buildings' complex and realistic forms.

The English in this document has been checked by at least two professional editors, both native speakers of English. For a certificate, please see: http://www.textcheck.com/certificate/RifLkg

Declaration of Competing Interest

None

Data availability

No data was used for the research described in the article.

Acknowledgments

This study was carried out with the support of 'R&D Program for Forest Science Technology (Project No. 2022428C10-2324-0802)' provided by Korea Forest Service (Korea Forestry Promotion Institute) and the Korea Meteorological Administration Research and Development Program under Grant KMI2021-03511.

Supplementary materials

Supplementary material associated with this article can be found, in the online version, at doi:10.1016/j.scs.2023.104537.

References

Abhijith, K. V., Kumar, P., Gallagher, J., McNabola, A., Baldauf, R., Pilla, F., & Pulvirenti, B. (2017). Air pollution abatement performances of green infrastructure in open road and built-up street canyon environments–A review. *Atmospheric Environment, 162*, 71–86.

Addepalli, B., & Pardyjak, E. R. (2013). Investigation of the flow structure in step-up street canyons—mean flow and turbulence statistics. *Boundary-layer Meteorology, 148*(1), 133–155.

Aflaki, A., Mirnezhad, M., Ghaffarianhoseini, A., Ghaffarianhoseini, A., Omrany, H., Wang, Z. H., & Akbari, H. (2017). Urban heat island mitigation strategies: A state-of-the-art review on Kuala Lumpur, Singapore and Hong Kong. *Cities, 62*, 131–145.

Baik, J. J., Kang, Y. S., & Kim, J. J. (2007). Modeling reactive pollutant dispersion in an urban street canyon. *Atmospheric Environment, 41*(5), 934–949.

Baik, J. J., & Kim, J. J. (1999). A numerical study of flow and pollutant dispersion characteristics in urban street canyons. *Journal of Applied Meteorology and Climatology, 38*(11), 1576–1589.

Balczó, M., Gromke, C., & Ruck, B. (2009). Numerical modeling of flow and pollutant dispersion in street canyons with tree planting. *Meteorologische Zeitschrift*.

Barwise, Y., & Kumar, P. (2020). Designing vegetation barriers for urban air pollution abatement: A practical review for appropriate plant species selection. *Npj Climate and Atmospheric Science, 3*(1), 12.

Bird, P. R. (1998). Tree windbreaks and shelter benefits to pasture in temperate grazing systems. *Agroforestry Systems*.

Brandle, J. R., Hodges, L., & Zhou, X. H. (2004). Windbreaks in North American agricultural systems. *Agroforestry Systems*.

Boeri, S. (2015). A vertical forest: Instructions booklet for the prototype of a forest city = Un bosco verticale: Libretto di istruzioni per il prototipo di una città foresta. Musante, G., Muzzonigro, A., Eds.

Buccolieri, R., Santiago, J. L., Rivas, E., & Sanchez, B. (2018). Review on urban tree modelling in CFD simulations: Aerodynamic, deposition and thermal effects. *Urban Forestry & Urban Greening, 31*, 212–220.

Chen, T., Yang, H., Chen, G., Lam, C. K. C., Hang, J., Wang, X., Liu, Y., & Ling, H. (2021). Integrated impacts of tree planting and aspect ratios on thermal environment in street canyons by scaled outdoor experiments. *Science of The Total Environment, 764*, Article 142920.

Claus, K., & Rousseau, S. (2012). Public versus private incentives to invest in green roofs: A cost benefit analysis for Flanders. *Urban Forestry & Urban Greening, 11*(4), 417–425.

Fellini, S., Ridolfi, L., & Salizzoni, P. (2020). Street canyon ventilation: Combined effect of cross-section geometry and wall heating. *Quarterly Journal of the Royal Meteorological Society, 146*(730), 2347–2367.

Foster, J., Lowe, A., & Winkelman, S. (2011). The value of green infrastructure for urban climate adaptation. *Center for Clean Air Policy, 750*(1), 1–52.

Gago, E. J., Roldan, J., Pacheco-Torres, R., & Ordóñez, J. (2013). The city and urban heat islands: A review of strategies to mitigate adverse effects. *Renewable and Sustainable Energy Reviews, 25*, 749–758.

Gallagher, J., Baldauf, R., Fuller, C. H., Kumar, P., Gill, L. W., & McNabola, A. (2015). Passive methods for improving air quality in the built environment: A review of porous and solid barriers. *Atmospheric Environment, 120*, 61–70.

Giardina, M., & Buffa, P. (2018). A new approach for modeling dry deposition velocity of particles. *Atmospheric Environment, 180*, 11–22.

Green, S. R. (1992). Modeling turbulent air flow in a stand of widely-spaced trees. *PHOENICS Journal of Computational Fluid Dynamics and its Applications, 5*, 294–312.

Gromke, C., Buccolieri, R., Di Sabatino, S., & Ruck, B. (2008). Dispersion study in a street canyon with tree planting by means of wind tunnel and numerical investigations–evaluation of CFD data with experimental data. *Atmospheric Environment, 42*(37), 8640–8650.

Gromke, C., & Blocken, B. (2015). Influence of avenue-trees on air quality at the urban neighborhood scale. Part I: Quality assurance studies and turbulent Schmidt number analysis for RANS CFD simulations. *Environmental Pollution, 196*, 214–223.

Hewitt, C. N., Ashworth, K., & MacKenzie, A. R. (2020). Using green infrastructure to improve urban air quality (GI4AQ). *Ambio, 49*(1), 62–73.

Huang, C. W., Lin, M. Y., Khlystov, A., & Katul, G. (2013). The effects of leaf area density variation on the particle collection efficiency in the size range of ultrafine particles (UFP). *Environmental Science & Technology, 47*(20), 11607–11615.

Irga, P. J., Burchett, M. D., & Torpy, F. R. (2015). Does urban forestry have a quantitative effect on ambient air quality in an urban environment? *Atmospheric Environment, 120*, 173–181.

Irga, P. J., Braun, J. T., Douglas, A. N. J., Pettit, T., Fujiwara, S., Burchett, M. D., & Torpy, F. R. (2017). The distribution of green walls and green roofs throughout Australia: Do policy instruments influence the frequency of projects? *Urban Forestry & Urban Greening, 24*, 164–174.

Kang, G., Kim, J.-J., Kim, D. J., Choi, W., & Park, S. J. (2017). Development of a computational fluid dynamics model with tree drag parameterizations: Application to pedestrian wind comfort in an urban area. *Building and Environment*.

Kang, G., Kim, J.-J., & Choi, W. (2020). Computational fluid dynamics simulation of tree effects on pedestrian wind comfort in an urban area. *Sustainable Cities and Society, 56*, Article 102086.

Kim, J. J., & Baik, J. J. (1999). A numerical study of thermal effects on flow and pollutant dispersion in urban street canyons. *Journal of Applied Meteorology, 38*(9), 1249–1261.

Kim, J. J., & Baik, J. J. (2004). A numerical study of the effects of ambient wind direction on flow and dispersion in urban street canyons using the RNG k–ε turbulence model. *Atmospheric Environment, 38*(19), 3039–3048.

Kim, M. J., Park, R. J., & Kim, J. J. (2012). Urban air quality modeling with full O3–NOx–VOC chemistry: Implications for O3 and PM air quality in a street canyon. *Atmospheric Environment, 47*, 330–340.

... Kumar, P., Druckman, A., Gallagher, J., Gatersleben, B., Allison, S., Eisenman, T. S., & Morawska, L. (2019). The nexus between air pollution, green infrastructure and human health *Environment International, 133*, Article 105181

Kurotani, Y., Kiyota, N., & Kobayashi, S. (2001). *Windbreak effect of Tsujimatsu in Izomu Part 2, D-2* pp. 745–746). Architectural Institute of Japan.

Launder, B. E., & Spalding, D. B. (1974). The numerical computation of turbulent flows. *Computer Methods Applied Mechnical Engineering, 3*(1974), 269–289.

Lee, I. Y., & Park, H. M. (1994). Parameterization of the pollutant transport and dispersion in urban street canyons. *Atmospheric Environment, 28*(14), 2343–2349.

Li, H., Zhao, Y., Sützl, B., Kubilay, A., & Carmeliet, J. (2022). *Impact of green walls on ventilation and heat removal from street canyons: Coupling of thermal and aerodynamic resistance* (p. 214). Building and Environment.

Loomis, D., Grosse, Y., Lauby-Secretan, B., El Ghissassi, F., Bouvard, V., Benbrahim-Tallaa, L., et al. (2013). The carcinogenicity of outdoor air pollution. *Lancet Oncology, 14*(13), 1262.

McNabola, A., O'Luanaigh, N., Gallagher, J., & Gill, L. (2013). The development and assessment of an aspiration efficiency reducing system of air pollution control for particulate matter in building ventilation systems. *Energy and Buildings, 61*, 177–184.

Moonen, P., Gromke, C., & Dorer, V. (2013). Performance assessment of Large Eddy Simulation (LES) for modeling dispersion in an urban street canyon with tree planting. *Atmospheric Environment*.

Mukherjee, A., & Agrawal, M. (2017). A global perspective of fine particulate matter pollution and its health effects. *Reviews of Environmental Contamination and Toxicology, 244*, 5–51.

Neft, I., Scungio, M., Culver, N., & Singh, S. (2016). Simulations of aerosol filtration by vegetation: Validation of existing models with available lab data and application to near-roadway scenario. *Aerosol Science and Technology, 50*(9), 937–946.

Park, S. J., Choi, W., Kim, J. J., Kim, M. J., Park, R. J., Han, K. S., & Kang, G. (2016). Effects of building–roof cooling on the flow and dispersion of reactive pollutants in an idealized urban street canyon. *Building and Environment, 109*, 175–189.

Park, S. J., Kim, J. J., Choi, W., Kim, E. R., Song, C. K., & Pardyjak, E. R. (2020). Flow characteristics around step-up street canyons with various building aspect ratios. *Boundary-Layer Meteorology, 174*(3), 411–431.

Patankar, S. V. (2018). *Numerical heat transfer and fluid flow*. CRC Press.

Qi, Y., & Ishihara, T. (2018). Numerical study of turbulent flow fields around of a row of trees and an isolated building by using modified k-ε model and LES model. *Journal of Wind Engineering and Industrial Aerodynamics*.

Ries, K., & Eichhorn, J. (2001). Simulation of effects of vegetation on the dispersion of pollutants in street canyons. *Meteorologische Zeitschrift*.

Santiago, J. L., Rivas, E., Sanchez, B., Buccolieri, R., & Martin, F. (2017). The impact of planting trees on NOx concentrations: The case of the Plaza de la Cruz neighborhood in Pamplona (Spain). *Atmosphere, 8*(7), 131.

Su, C. W., Yuan, X., Tao, R., & Umar, M. (2021). Can new energy vehicles help to achieve carbon neutrality targets? *Journal of Environmental Management, 297*, Article 113348.

Tominaga, Y., & Stathopoulos, T. (2016). Ten questions concerning modeling of near-field pollutant dispersion in the built environment. *Building and Environment, 105*, 390–402.

Versteeg, H. K., & Malalasekera, W. (1995). *An introduction to computational fluid dynamics: The finite volume method* (pp. 198–203). Malaysia: Longman. and 243–244.

Vos, P. E., Maiheu, B., Vankerkom, J., & Janssen, S. (2013). Improving local air quality in cities: To tree or not to tree? *Environmental Pollution, 183*, 113–122.

World Health Organization. (2006). *Air quality guidelines: Global update 2005: Particulate matter, ozone, nitrogen dioxide, and sulfur dioxide*. World Health Organization.

Yakhot, V., Orszag, S. A., Thangam, S., Gatski, T. B., & Speziale, C. G. (1992). Development of turbulence models for shear flows by a double expansion technique. *Physics of Fluids A*.

Zhang, L., Gong, S., Padro, J., & Barrie, L. (2001). A size-segregated particle dry deposition scheme for an atmospheric aerosol module. *Atmospheric environment, 35*(3), 549–560.

Zhang, L., Zhang, Z., McNulty, S., & Wang, P. (2020). The mitigation strategy of automobile generated fine particle pollutants by applying vegetation configuration in a street-canyon. *Journal of Cleaner Production, 274*, Article 122941.